

The Force-Free Electrodynamics Method for Nonlinear Extrapolation from Vector Magnetograms

I. Contopoulos

© Springer

Abstract We present a new improved version of our force-free electrodynamics (FFE) numerical code in spherical coordinates that extrapolates the magnetic field in the inner solar corona from a photospheric vector magnetogram. The code satisfies the photospheric boundary condition and the condition $\nabla \cdot \mathbf{B} = 0$ to machine accuracy. The performance of our method is evaluated with standard convergence parameters, and is found to be comparable to that of other nonlinear force-free extrapolations.

Keywords: Active Regions, Magnetic Fields; Magnetic Fields, Corona;

1. Introduction

Force-free electrodynamics (hereafter FFE) is a formal name for time-dependent electromagnetism in an ideal plasma with negligible inertia and gas pressure ($\beta \approx 0$). The formalism of FFE has been developed for various relativistic astrophysical applications where the plasma supports electric currents and electric charges (pulsars, astrophysical jets, gamma-ray bursts, *etc.*). The equations of FFE are Maxwell's equations with nonzero electric currents,

$$\frac{\partial \mathbf{E}}{\partial t} = c \nabla \times \mathbf{B} - 4\pi \mathbf{J}, \quad \frac{\partial \mathbf{B}}{\partial t} = -c \nabla \times \mathbf{E}, \quad (1)$$

complemented by the divergence-free, ideal MHD, and force-free conditions

$$\nabla \cdot \mathbf{B} = 0, \quad \mathbf{E} \cdot \mathbf{B} = 0, \quad \rho_e \mathbf{E} + \frac{1}{c} \mathbf{J} \times \mathbf{B} = 0. \quad (2)$$

Here, \mathbf{J} and $\rho_e \equiv (4\pi)^{-1} \nabla \cdot \mathbf{E}$ are the electric current and charge densities, respectively. One can solve the above set of equations for \mathbf{J} and thus express the electric current density as a function of the electric and magnetic fields, namely

$$\mathbf{J} = \frac{c}{4\pi} \nabla \cdot \mathbf{E} \frac{\mathbf{E} \times \mathbf{B}}{B^2} + \frac{c}{4\pi} \frac{(\mathbf{B} \cdot \nabla \times \mathbf{B} - \mathbf{E} \cdot \nabla \times \mathbf{E})}{B^2} \mathbf{B} \quad (3)$$

Research Center for Astronomy and Applied Mathematics
(RCAAM), Academy of Athens, 4 Soranou Efessiou Str.,
Athens 11527, Greece, email: icontop@academyofathens.gr

(Gruzinov, 1999). One can then numerically integrate Maxwell's equations to follow the temporal evolution of any force-free ideal-MHD system from an initial to a final configuration. In the particular case when $\mathbf{E} \xrightarrow{t \rightarrow \infty} 0$, the final configuration is (in general) a non-linear force-free magnetostatic field, *i.e.* it satisfies the relations

$$\mathbf{J} = \frac{c}{4\pi} \nabla \times \mathbf{B} , \quad \nabla \cdot \mathbf{B} = 0 , \quad \mathbf{J} \times \mathbf{B} = 0 . \quad (4)$$

The FFE method has been applied successfully in two main astrophysical applications; pulsars (Spitkovsky, 2006; Kalapotharakos and Contopoulos, 2009), and the solar corona (Contopoulos, Kalapotharakos, and Georgoulis, 2011, hereafter CKG). The numerical codes developed for these problems are Cartesian finite-difference time-domain (FDTD) codes. They are based on the staggered mesh algorithm of Yee (1966) where in every computational cell, electric field components are defined in the middle of and along cell edges, whereas magnetic field components are defined in the middle of and perpendicular to cell faces. It is very important to notice that this prescription satisfies the divergence-free condition $\nabla \cdot \mathbf{B} = 0$ to machine accuracy. Kalapotharakos and Contopoulos (2009) introduced also an outer absorbing non-reflecting boundary condition in the form of a perfectly matched layer (PML). CKG implemented the FFE method in the study of the inner solar corona by evolving the photospheric boundary condition toward a given distribution for the radial component of the magnetic field. This is achieved with the introduction of photospheric electric fields which gradually die out as the required photospheric condition is approached. During that evolution, the FFE equations are numerically solved in the solar corona, and in the limit when electric fields die out everywhere, a non-linear force-free magnetostatic configuration emerges.

There are several problems with this approach: a) The method is based on knowledge only of the radial component of the photospheric magnetic field; therefore the final solution is not unique. Different initial conditions and different photospheric evolutionary paths yield different magnetostatic configurations. b) Numerical dissipation cannot be avoided, and therefore, the longer a particular implementation takes to converge to a certain acceptable accuracy, the smaller the final remaining magnetospheric electric current, and the closer the final solution approaches the potential (current-free) equilibrium. c) The numerical grid is Cartesian. This works well around the poles, but is unsuitable to appropriately model the solar photosphere in general.

For all of the above reasons, we decided to improve our code, and to incorporate the photospheric boundary condition supplied from a full vector magnetogram .

2. Implementation of the Vector Magnetogram Boundary Condition

The new improved version of our code is written in the natural coordinates for the solar corona, namely heliocentric spherical ones (r, θ, ϕ) . In order to satisfy the photospheric boundary condition exactly, we altogether skip the photospheric

relaxation algorithm described in CKG, and begin instead with the following ‘sea urchin’-like initial magnetic field configuration:

$$B_r(r, \theta, \phi; t = 0) = \mathcal{B}_r(\theta, \phi)(r_\odot/r)^2 ,$$

$$B_\theta(r_\odot, \theta, \phi; t = 0) = \mathcal{B}_\theta(\theta, \phi) ,$$

$$B_\phi(r_\odot, \theta, \phi; t = 0) = \mathcal{B}_\phi(\theta, \phi) , \quad \text{and}$$

$$B_\theta(r > r_\odot, \theta, \phi; t = 0) = B_\phi(r > r_\odot, \theta, \phi; t = 0) = 0 .$$

This configuration is obviously divergence-free, and satisfies the photospheric boundary condition $\mathbf{B}(r_\odot, \theta, \phi) \equiv \mathcal{B}(\theta, \phi)$ exactly. We also set $\mathbf{E} = 0$ on the photosphere at all times. Notice that the algorithm that we implement (Yee, 1966) satisfies $\nabla \cdot \mathbf{B} = 0$ to machine accuracy *only if the initial configuration is divergence-free*. In other words, the algorithm does not implement the divergence-free condition. It inherits and preserves it. Notice also that the initial configuration is filled with electric currents in the θ - and ϕ -directions, but not in the radial one.

We then proceed as in CKG with a numerical integration of Equations (1) and (3). Initially, the magnetic field configuration becomes torn through numerical reconnection. The sea urchin-like configuration gradually disappears. Transient electromagnetic-type waves travel through the integration volume and when they reach the outer radial boundary they are absorbed by the PML (see below). Eventually, this transient activity dies out, electric fields are observed to converge to $\mathbf{E} \xrightarrow{t \rightarrow \infty} 0$, and a non-linear force-free magnetostatic equilibrium is gradually reached. Notice that during this evolution, the divergence-free and vector photospheric boundary conditions are everywhere satisfied.

Our method can be implemented in both global and local magnetic field extrapolations. In global extrapolations, the numerical integration volume lies between an inner radius $r_{\text{in}} = r_\odot$ (the photosphere), and an outer radius r_{out} that corresponds to the distance beyond which the solar wind becomes dynamically important. The integration volume corresponds to the lower solar corona where we assume that force-free magnetostatic conditions apply to a certain extent. In the test simulations presented in the next section, we took $r_{\text{out}} = 2r_\odot$. In general, r_{out} may vary between $2r_\odot$ and $3r_\odot$, depending on the strength of the solar wind. Beyond that radius, we implement a PML non-reflecting absorbing layer of thickness $0.5r_\odot$. In the polar direction, the simulation is limited between a minimum and a maximum polar angle $\theta_{\text{min}} = 20^\circ$ and $\theta_{\text{max}} = 160^\circ$, in order to avoid the polar singularity of the spherical coordinate system. In realistic solar coronal magnetic field configurations, the polar regions are covered by coronal holes, and therefore, their exclusion does not significantly affect the extrapolation. Finally, in the azimuthal direction we implement periodic boundary conditions. The test simulations presented in the next section are all global extrapolations except for the last one that is limited in the azimuthal extent.

3. Evaluation of Numerical Code

In order to evaluate the performance of our code, we implement vector photospheric boundary conditions derived from standard solutions that are used as benchmarks, and evaluate the convergence of the extrapolation based on standard convergence parameters introduced in Wheatland, Sturrock, and Roumeliotis (2000), Schrijver *et al.* (2006), and Amari, Boulmezaoud, and Aly (2006) (see the Appendix for their detailed expressions). The benchmark solutions are known either analytically (dipole), or quasi-analytically (Low and Lou, 1990, hereafter LL). In most previous implementations, benchmark boundary conditions on the xy -plane were obtained by displacing the LL solution some distance l below the xy -plane, and by rotating it by an angle Φ with respect to the y -axis (see the original LL paper for details). To the best of our knowledge, the only previous work where the LL solutions were applied in a coronal magnetic field configuration over a curved photospheric boundary is Tadesse, Wiegmann, and Inhester (2009). We thus decided, for the sake of comparison, to also implement their boundary condition. We investigated the following test cases:

- Case DF: a dipole magnetic field off-axis by $0.5r_\odot$
- Case LL11: LL solution with $n = 1$, $m = 1$, $l = 0.25r_\odot$ (displacement below the xy -plane), $\Phi = \pi/10$ (as in Tadesse, Wiegmann, and Inhester, 2009)
- Case LL13: LL solution with $n = 1$, $m = 3$, $l = 0.1r_\odot$ (displacement below the yz -plane), $\Phi = 4\pi/5$
- Case LL31: LL solution with $n = 3$, $m = 1$, $l = 0.1r_\odot$ (displacement below the yz -plane), $\Phi = 4\pi/5$

Case DF is current-free (potential), but the LL solutions are not. The radial resolution of these particular simulations is $0.1r_\odot$, and the angular resolution $4^\circ \times 4^\circ$ (heliocentric). We set $\theta_{\min} = 20^\circ$ and $\theta_{\max} = 160^\circ$. Our computational grid in (r, θ, ϕ) has a resolution of $10 \times 34 \times 90$.

In Table 1, we plot the values of our convergence parameters in a subregion of our computational volume (we chose $r_\odot < r < 1.5r_\odot$, $30^\circ < \theta < 60^\circ$, $30^\circ < \phi < 60^\circ$) in the force-free extrapolations obtained for the above four benchmark solutions. The first four parameters characterize the convergence to the benchmark solution (unity corresponds to a perfect match). The last two parameters characterize how well the extrapolation satisfies the force-free and divergence-free conditions respectively. In all cases, the divergence-free and boundary conditions are satisfied to machine accuracy. The force-free condition is also very important for us. We evolve the numerical simulation till we obtain a minimum of the parameter CW_{\sin} at a level roughly below 0.15. This guarantees that the solutions that we present are indeed non-linear force-free magnetostatic configurations that satisfy the given vector magnetogram boundary conditions. Notice that the force-free parameter (Equation (10)) does not apply in potential extrapolations where $J \rightarrow 0$.

The performance of our code is satisfactory, which suggests that the present numerical method is promising. In some benchmark cases, it outperforms existing Cartesian grid extrapolations (see *e.g.* Jiang and Feng, 2012), and is certainly on a par with the spherical grid extrapolation of Tadesse, Wiegmann, and Inhester

Table 1. Convergence parameters for various benchmark extrapolations on a computational grid with a resolution in (r, θ, ϕ) of $10 \times 34 \times 90$.

Case	C_{vec}	C_{CS}	E'_n	E'_m	CWsin	f	Comments
DF	0.989	0.986	0.845	0.821	...	10^{-9}	Current-free
LL11	0.993	0.987	0.895	0.873	0.087	10^{-8}	as in Tadesse <i>et al.</i> (2009)
LL13	0.915	0.924	0.403	0.389	0.109	10^{-8}	Different solution
LL31	0.981	0.978	0.772	0.715	0.110	10^{-7}	Non-global in azimuth

(2009) (compare our case LL11 with Case 1 in their low resolution grid). In some cases, though, the resulting extrapolation does not converge to the benchmark solution in the volume under investigation, as manifested for example in case LL13 where two convergence parameters differ significantly from unity. We offer two possible explanations for this result: a) An extrapolation where a significant amount of magnetic flux crosses the outer boundaries of the numerical integration region is influenced by the presence of those boundaries more than another extrapolation where most magnetic field lines are contained within the computational volume. b) A non-linear extrapolation is not unique when current sheets are allowed to develop in the solution. This needs to be confirmed with more detailed evolutionary full MHD extrapolations. Notice that our force-free code handles current sheets as tangential magnetic field discontinuities with $|B|$ continuous everywhere (see Contopoulos, Kazanas, and Fendt (1999) and Kalapotharakos and Contopoulos (2009) for details). Finally, we noticed that in a few cases the extrapolation did not converge, probably due to an incompatibility between the photospheric vector boundary condition and the conditions at the outer boundaries of the computational volume. As an example, the global extrapolation failed in case LL31; however, when we limited the azimuthal integration region to $20^\circ < \phi < 160^\circ$ the extrapolation was successful. The convergence properties of our method certainly need further investigation.

The resulting solutions can be visually compared with the corresponding benchmark solutions in Figure 1 where field lines originating from the same photospheric positions are plotted. We notice that the extrapolation produces field lines that are visibly more stretched-out radially than the benchmark solution. This is particularly obvious in the case of a current-free displaced dipole and in the field lines that cross the outer radial boundary at $r = 2r_\odot$. This result is an artefact of our method that qualitatively mimics the effect of the solar wind beyond the outer radial distance.

4. Prospects for the Future

The implementation of the photospheric boundary condition from full vector magnetograms in the new version of our code improves the nonlinear force-free extrapolation of CKG in several respects. Firstly, it generates a more physical

solution (closer to reality). Secondly, it resolves the non-uniqueness problem of the original version where different initial conditions and different photospheric evolutions yielded different magnetostatic configurations. And thirdly, it does not allow the extrapolation to ‘degenerate’ to the potential configuration. Our test runs suggest that the method is promising, as it outperforms existing extrapolations in some benchmark cases. We therefore expect that it has significant potential in the study of the lower solar corona and of individual active regions.

We are currently running our code on a desktop PC. Our global coronal magnetic field extrapolations were obtained with a heliocentric angular resolution of $4^\circ \times 4^\circ$, on an (r, θ, ϕ) spherical computational grid of $10 \times 34 \times 90$, but this can certainly be improved. Our goal is to parallelize the code to run in a supercomputer. In a future implementation we will also improve the performance of the PML outer boundary by fine-tuning its parameters (our current implementation allows for some minor amount of reflection of transient electromagnetic-type waves).

An ambitious goal is to apply our method to investigate particular active regions with minimum influence from the simulation outer boundaries on the extrapolation. As we saw, the effect of the outer boundaries differs from case to case, and we can only give an empirical rule that the assumed volume must be about double the size of the particular volume under investigation in all directions (radial, polar, and azimuthal). Our goal for the future is to solve for the magnetic field of a particular region as part of (*i.e.* together with) a global coronal magnetic field extrapolation. This can be achieved in practice by introducing adaptive mesh refinement (AMR) around the region under investigation and around neighboring regions that may interact with that region. In practice, we will need about five adaption levels in order to match the available heliocentric angular resolution in particular active regions (about $0.05^\circ \times 0.05^\circ$) to the resolution that can be practically achieved on a single PC in a global magnetic field extrapolation (about $2^\circ \times 2^\circ$). Thus, the extrapolation for one particular active region will take into account the presence of neighboring active regions, as well as the global coronal magnetic field structure.

One final goal is to introduce finite (non-infinite) conductivity σ in the code by modifying the FFE expression for the electric current density as

$$\mathbf{J} = \rho_e \frac{\mathbf{E} \times \mathbf{B}}{B^2} + \sigma \mathbf{B} , \quad (5)$$

We plan to investigate various nonlinear prescriptions for σ (*e.g.* weighted by the value of J) as we are currently doing in our study of the pulsar magnetosphere (see Kalapotharakos *et al.* (2012) for details). Finite conductivity will allow for the presence of electric fields along the magnetic field, *i.e.* it will introduce volume energy dissipation $\mathbf{J} \cdot \mathbf{E}$. We expect that this approach will give us direct hints about where and how magnetic field energy is released in the solar corona.

Acknowledgements This work was supported in part by the Research Commission of the Academy of Athens.

Appendix

Convergence Parameters

We evaluate the following parameters introduced in Wheatland, Sturrock, and Roumeliotis (2000), Schrijver *et al.* (2006), and Amari, Boulmezaoud, and Aly (2006): the vector correlation C_{vec}

$$C_{\text{vec}} \equiv \sum_i \mathbf{B}_i \cdot \mathbf{b}_i / \left(\sum_i |\mathbf{B}_i|^2 \sum_i |\mathbf{b}_i|^2 \right)^{1/2}, \quad (6)$$

the parameter C_{CS}

$$C_{\text{CS}} \equiv \frac{1}{N} \sum_i \frac{\mathbf{B}_i \cdot \mathbf{b}_i}{|\mathbf{B}_i| |\mathbf{b}_i|}, \quad (7)$$

and the normalized and mean vector error E'_n and E'_m

$$E'_n \equiv 1 - \sum_i |\mathbf{B}_i - \mathbf{b}_i| / \sum_i |\mathbf{B}_i|, \quad (8)$$

$$E'_m \equiv 1 - \frac{1}{N} \sum_i \frac{|\mathbf{B}_i - \mathbf{b}_i|}{|\mathbf{B}_i|}, \quad (9)$$

where \mathbf{B}_i and \mathbf{b}_i are the extrapolation and reference fields, respectively, i denotes grid points, and N is the total number of grid points in the sub-region of our simulation where we evaluate the convergence of the code. The force-free and divergence-free conditions are estimated using the following parameters:

$$\text{CWsin} \equiv \frac{\sum_i |\mathbf{J}_i \times \mathbf{B}_i| / |\mathbf{B}_i|}{\sum_i |\mathbf{J}_i|}, \quad (10)$$

$$f \equiv \frac{1}{N} \sum_i \frac{(\nabla \cdot \mathbf{B})_i}{6|\mathbf{B}_i|/d}, \quad (11)$$

where d is the minimum grid spacing. Those may be evaluated over the total integration volume, or over a smaller internal volume.

References

- Amari, T., Boulmezaoud, T.Z., Aly, J.J.: 2006, Well posed reconstruction of the solar coronal magnetic field. *Astron. Astrophys.* **446**, 691–705. doi:10.1051/0004-6361:20054076.
- Contopoulos, I., Kalapotharakos, C., Georgoulis, M.K.: 2011, Nonlinear force-free reconstruction of the global solar magnetic field: Methodology. *Solar Phys.* **269**, 351–365. doi:10.1007/s11207-011-9713-x.
- Contopoulos, I., Kazanas, D., Fendt, C.: 1999, The axisymmetric pulsar magnetosphere. *Astrophys. J.* **511**, 351–358. doi:10.1086/306652.
- Gruzinov, A.: 1999, Stability in force-free electrodynamics. *ArXiv Astrophysics e-prints*.

-
- Jiang, C., Feng, X.: 2012, A new implementation of the magnetohydrodynamics-relaxation method for nonlinear force-free field extrapolation in the solar corona. *Astrophys. J.* **749**, 135. doi:10.1088/0004-637X/749/2/135.
- Kalapothisarakos, C., Contopoulos, I.: 2009, Three-dimensional numerical simulations of the pulsar magnetosphere: preliminary results. *Astron. Astrophys.* **496**, 495–502. doi:10.1051/0004-6361/200810281.
- Kalapothisarakos, C., Kazanas, D., Harding, A., Contopoulos, I.: 2012, Toward a realistic pulsar magnetosphere. *Astrophys. J.* **749**, 2. doi:10.1088/0004-637X/749/1/2.
- Low, B.C., Lou, Y.Q.: 1990, Modeling solar force-free magnetic fields. *Astrophys. J.* **352**, 343–352. doi:10.1086/168541.
- Schrijver, C.J., De Rosa, M.L., Metcalf, T.R., Liu, Y., McTiernan, J., Régnier, S., Valori, G., Wheatland, M.S., Wiegmann, T.: 2006, Nonlinear force-free modeling of coronal magnetic fields part I: A quantitative comparison of methods. *Solar Phys.* **235**, 161–190. doi:10.1007/s11207-006-0068-7.
- Spitkovsky, A.: 2006, Time-dependent force-free pulsar magnetospheres: Axisymmetric and oblique rotators. *Astrophys. J. Lett.* **648**, L51–L54. doi:10.1086/507518.
- Tadesse, T., Wiegmann, T., Inhester, B.: 2009, Nonlinear force-free coronal magnetic field modelling and preprocessing of vector magnetograms in spherical geometry. *Astron. Astrophys.* **508**, 421–432. doi:10.1051/0004-6361/200912529.
- Wheatland, M.S., Sturrock, P.A., Roumeliotis, G.: 2000, An optimization approach to reconstructing force-free fields. *Astrophys. J.* **540**, 1150–1155. doi:10.1086/309355.
- Yee, K.: 1966, Numerical solution of initial boundary value problems involving Maxwell’s equations in isotropic media. *IEEE Trans. Antennas Propag.* **14**, 302–307. doi:10.1109/TAP.1966.1138693.

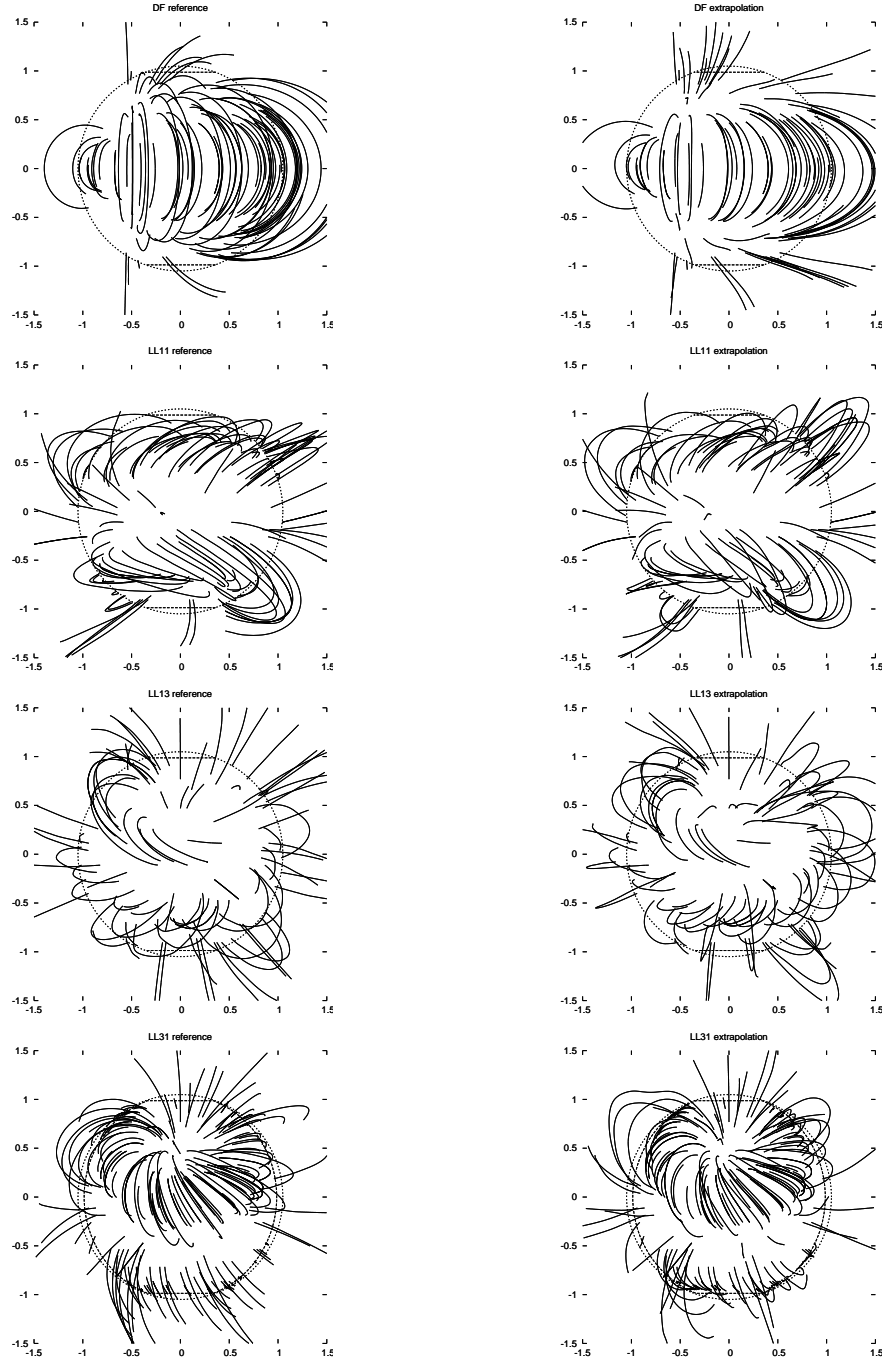


Figure 1. Comparison between benchmark solutions (left) and their corresponding extrapolations (right) for the four cases of Table 1. In case LL11, the disk center corresponds to 180° longitude. In the other three cases, it corresponds to 90° longitude. Dashed lines mark the simulation photospheric boundaries.

